



# Landslide and Soil Erosion Inventory Mapping Based on High-Resolution Remote Sensing Data: A Case Study from Istria (Croatia)

Sanja Bernat Gazibara, Petra Jagodnik, Hrvoje Lukačić, Marko Sinčić, Martin Krkač, Gabrijela Šarić, Željko Arbanas, and Snježana Mihalić Arbanas

## Abstract

The central part of the Istrian Peninsula (Croatia) is the area of the Eocene flysch basin, i.e. “Gray Istria, which is prone to weathering and active geomorphological processes. The high erodibility of the Istrian marls led to the formation of steep barren slopes and badlands exceptionally susceptible to slope movements. This research presents the application of high-resolution remote sensing data, i.e., Light Detection and Ranging (LiDAR) data and orthophoto images, for landform mapping at a large scale (1:500). Visual interpretation of remote sensing data was done for the pilot area (20 km<sup>2</sup>) near City of Buzet to produce detailed inventory maps for implementation in the spatial planning system. There is a lack of detailed inventory maps because systematic mapping was not performed for any part of Istria until the scientific research project *LandSlidePlan* (HRZZ IP-2019-04-9900), funded by the Croatian Science Foundation. After preliminary visual interpretation of LiDAR DTM and field verifications, it was concluded that four types of landforms could be mapped, i.e. badlands, gully and combined erosion, unstable slopes and landslides. The research objective is to show the representative examples and potential of direct and unambiguous identification and mapping of small and shallow landslides and soil erosion processes based on the visual interpretation of high-resolution remote sensing data in flysch-type rock.

## Keywords

Landslides · Soil erosion · Inventory mapping · LiDAR

S. Bernat Gazibara (✉) · H. Lukačić · M. Sinčić · M. Krkač · G. Šarić · S. Mihalić Arbanas

University of Zagreb Faculty of Mining, Geology and Petroleum Engineering, Zagreb, Croatia  
e-mail: [sanja.bernat@rgn.unizg.hr](mailto:sanja.bernat@rgn.unizg.hr)

P. Jagodnik · Ž. Arbanas  
University of Rijeka Faculty of Civil Engineering, Rijeka, Croatia

## 1 Introduction

Inventory mapping of slope processes presents essential input parameters for multiple spatial analyses such as landslide or erosion susceptibility, hazard, and risk assessment (Guzzetti et al. 2000; van Westen et al. 2006), especially in the case of large-scale hazard zoning (Sinčić et al. 2022). However, the traditional landslide and erosional inventory mapping methods include field mapping and interpretation of aerial photos and satellite images, which produces a limited amount of data in case of an inaccessible and overgrown area. Therefore, the LiDAR data is the only appropriate remote sensing tool for landslide and soil erosion mapping in a forest or densely vegetated areas. The landslide maps obtained through the visual analysis of LiDAR-derived DTMs have better landslide area statistics and completeness than the inventories obtained through field mapping or the interpretation of aerial photographs (Eeckhaut et al. 2007).

One of the priorities for an action plan in the Sendai Framework for Disaster Risk Reduction 2015–2030 (UN 2015) is understanding disaster risk in all its dimensions and disseminating location-based information to decision-makers, the general public, and at-risk communities. Therefore, the most critical risk reduction measure and mitigation of the geohazards’ consequences is creating inventory and prognostic maps that should be implemented into the spatial planning system for defining building conditions or restricting development in erosion or landslide-prone areas. The scientific research project *Methodology development for landslide susceptibility assessment for land-use planning based on LiDAR technology* (LandSlidePlan, HRZZ IP-2019-04-9900), funded by the Croatian Science Foundation (Bernat Gazibara et al. 2022), deals with inventory mapping of small and shallow landslides and presents innovative approaches to scientific research of landslide susceptibility assessment using LiDAR technology. Among other study areas, selected based on geological settings and degree

of urbanisation, the landslide maps will be developed for the pilot area in the central part of the Istrian Peninsula (Croatia).

## 2 Study Area

The Istrian peninsula is a geomorphological unit separated from the interior by the limestone mountains of the Čićarija Mt. Istria is geomorphologically composed of a hilly northern edge (White Istria), lower flysch hills (Gray Istria) and low limestone plateaus (Red Istria). “Gray Istria” is in the inland of the Istrian peninsula, where a more continental and humid climate prevails. Based on the precipitation data recorded at the Lanišće weather station (NE border of the Istrian flysch basin) for the past 49 years (from 1961 to 2010), this area received mean annual precipitation (MAP) of 1774.3 mm.

The study area (19.96 km<sup>2</sup>) is located in the northern part of Istrian County, in Gray Istria, and it includes the part of the City of Buzet between the valley of the river Mirna in the north and the accumulation Butoniga in the south. From the

geomorphological standpoint, it is a predominantly hilly area with most terrain steeper than 12°. Approximately 2.6% of the study area has slope angles less than 2°, 9.7% between 2–5°, 25.5% between 5–12°, 45.5% between 12–32°, 16.1% between 32–55° and 1.1% steeper than 55° (Fig. 1a).

According to the Basic geological map of Croatia with a scale of 1:100,000, most of the study area is composed of Middle Eocene sediments (Fig. 1b). Those are represented by the alteration of sandstones and marls, also known as flysch deposits, with thicknesses ranging from 0.3–7 m (Pleničar et al. 1969). Bergant et al. (2003) state that Flysch deposits can be divided into upper and lower parts. The lower part of the flysch complex is mainly composed of the interbedding of marls and carbonate lithological members with occasional carbonate megalayers. On the other hand, the upper part of the Flysch complex is mainly composed of carbonate turbidite sediments which appear in very thin layers. Alongside the Middle Eocene sediments study area comprises Alluvium deposits as the youngest lithological member and Nummulitic and Foraminifera Limestones as the oldest lithological member.

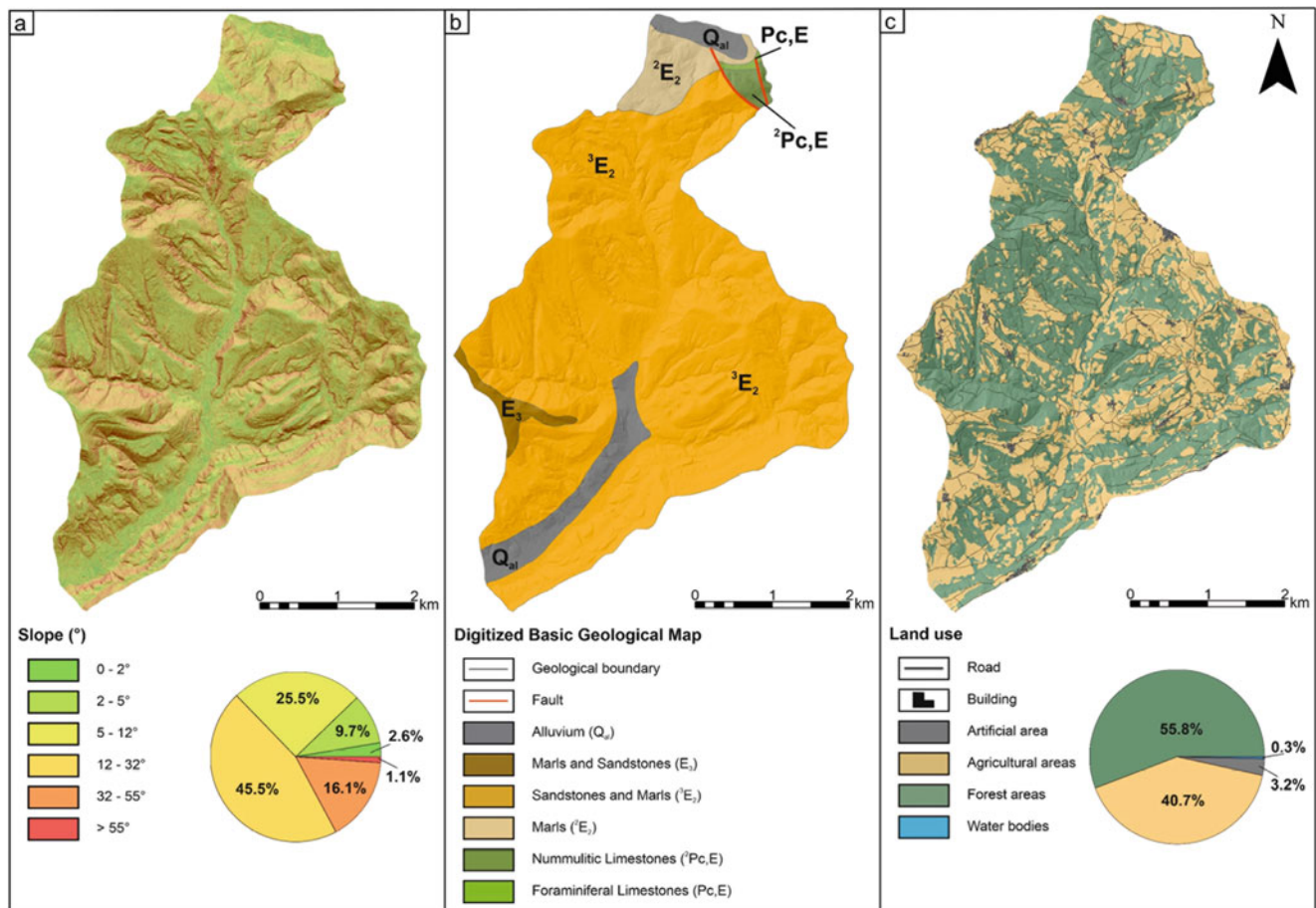


**Fig. 1** Study area location and characteristics: (a) slope distribution; (b) geology; (c) land-use

In Sinčić et al. (2022), a detailed land use classification based on high-resolution orthophoto images was performed for the study area. As shown in Fig. 1c, 55.8% of the study area is covered by forests, 40.7% is an agricultural area, 3.2% is artificial (urban), and 0.3% represents water bodies. Although the population density is low, the revitalisation of old and abundant villages and construction outside of the areas defined in the spatial plans due to tourism development is present in the interior parts of the Istrian peninsula.

The central part of Istria is characterised by moderate dissection (100–300 m), which is a consequence of the high erodibility and low durability of flysch sediments and the reason for the frequent occurrence of intense exogenetic processes, such as sliding (Arbanas et al. 1999; Dugonjić Jovančević and Arbanas 2012; Arbanas et al. 2014), gully erosion and badland formation (Gulam et al. 2014.). In addition, more intensive weathering and selective erosion of less-durable marls compared with sandstones enable the development of deeper weathering profiles with up to 10 m of weathered rock mass (Vivoda Prodan and Arbanas 2016).

Sliding is most often in weathered Eocene flysch-like deposits and on contacts between weathered and fresh flysch-type rock, especially at places of concentrated flows of superficial water (e.g., near roads), which typically cause small and shallow landslides (Dugonjić Jovančević and Arbanas 2012). Also, block translational landslides are possible (Arbanas et al. 2010; Mihalić et al. 2011). Landslides are mostly small to medium-sized (Fig. 2a, b), with sliding surfaces at depths of several meters to a maximum of 15 m triggered mostly by precipitations and human activity. Dugonjić Jovančević et al. analysed 19 landslides recorded as singular phenomena that occurred from 1979 through 2010, and the general conclusion is that long rainfall periods are crucial for initiating landslides. In contrast, short rainfalls have a significant influence on erosion. Moreover, debris flows (Arbanas et al. 2006), rock falls, and toppling (Fig. 2c, d) also become active under the influence of heavy rainfall and superficial flows.

Since 2008, the landslide database for the “Gray Istria” was conducted by the Department of Hydrotechnics and Geotechnics, Faculty of Civil Engineering, University of Rijeka, using documentation collected from the department’s archives and the archives of the Istrian County Roads Office and the Civil Engineering Institute of Croatia. The collected data for the studied landslides contain basic information about the location, type, dimensions and time of occurrence and other data from geological and geotechnical studies, laboratory test reports, remediation designs, etc. However, there is a lack of detailed landslide inventories because systematic inventory mapping was not performed for any part of Istria until today.

Badland formations (Fig. 3) in the central part of Istria are predefined by the combination of specific lithology, i.e. Eocene flysch deposits, and climate. However, according to Gulam et al. (2014), the most important factor in badland development and formation is the close contact of the channel flow with the accumulated material at the badland slope foot. Also, badlands in central Istria are very small, susceptible to slope movements and characterised by sparse or no vegetation. The most extensive single badland area has an area of 0.08 km<sup>2</sup>, according to the badland inventory map made by Gulam et al. (2014), based on visual identification and mapping of the orthophoto images on a scale of 1:5.000. Existing inventory covers approx. 500 km<sup>2</sup> in the central part of Istria, and the badland area covers 2.2% of the total research area. However, there is a lack of previous investigations on other soil erosion processes in the central part of Istria, such as gully or sheet erosion, and these processes were never systematically mapped.

### 3 Remote Sensing Data

Remote sensing data for the study area were acquired in the framework of the project “*Methodology development for landslide susceptibility assessment for land-use planning based on LiDAR technology (LandSlidePlan IP-2019-04-9900)*” funded by the Croatian Science Foundation (Bernat Gazibara et al. 2022).

LiDAR scanning using an Airborne laser scanning system (ALS) was undertaken in March 2020 using Reigl LMS-Q780 long-range airborne laser scanner coupled with a high-resolution Hasselblad camera at the average altitude of 700 m a.s.l.. LiDAR system used in this study acquires data at the pulse rate of 400 kHz and horizontal surface accuracy of 3 cm (XY plane) and vertical accuracy of 4 cm (Z-direction). Final Point Cloud has approx. 623 million points, with an average point density of 16,09 pt./m<sup>2</sup> resulting in average point spacing of 0.18 cm. Additionally, the final Point Cloud was classified into four distinct classes: (i) default unclassified points, (ii) ground bare earth points, (iii) vegetation, and (iv) noise. Based on the classified Point Cloud bare-earth DEM was generated using kriging interpolation method resulting in a spatial resolution of 30 cm.

For the purpose of landslide and soil erosion inventory mapping morphometric derivative maps were derived from a 30 cm resolution digital terrain model (DTM) using ArcGIS 10.8. software. A total of four types of morphometric derivatives were used; (i) hillshade map, (ii) slope map, (iii) roughness map (Surface/Area Ratio, SAR), and (iv) stream power index map (SPI).

Hillshade map represents a pseudo-three-dimensional visualisation of the terrain surface used for the visual



**Fig. 2** Badlands in the Istrian flysch area

interpretation of morphological terrain characteristics (Guzzetti et al. 2012). The map was derived using ArcGIS 10.8. Spatial Analyst extension Hillshade by simulating the illumination conditions that are defined by the azimuth of the light source ( $0^\circ$  to  $360^\circ$ ) and the angle of incidence of light rays ( $0^\circ$  to  $90^\circ$ ). The resulting map has the value of surface brightness for each cell ranging from 0 to 254, depending on the illumination conditions (Jenness 2007). The final hillshade map was derived using illumination parameters  $315^\circ/45^\circ$  and  $45^\circ/45^\circ$ .

Slope map represents the spatial distribution of the terrain slope angle (gradient or steepness) ranging from  $0^\circ$ - $90^\circ$ . As

well as the hillshade map the slope map enables the identification of characteristic geomorphological elements such as landslide and erosion boundaries (Ardizzone et al. 2007). The map was derived using ArcGIS 10.8. Spatial Analyst extension Slope which calculates the average slope angle value using a 3 by 3 cell moving window to process the data for the same (central) pixel and the eight surrounding pixels' angle.

Terrain roughness map represents the local variability in the slope angle, terrain elevation, and slope orientation. For the purpose of the landslide and erosion inventory mapping Surface/Area Ratio (SAR) map proposed by Berry (2002)



**Fig. 3** Landslides activated in December 2020 in the Istrian flysch area

was used. The map represents the ratio between 2D and 3D terrain maps using the following expression (Berry 2002):

$$\text{SAR} = \frac{c^2}{\cos\left(\text{slp}\left(\frac{\pi}{180}\right)\right)} \quad (1)$$

where  $c$  is the DTM cell size,  $\text{slp}$  is the slope map in degrees derived from the LiDAR DTM. The final SAR map was classified into two categories using the quantile classification method.

Stream power index (SPI) map represents the erosive power of the surface water runoff (Moore et al. 1991). For the calculation of the SPI, it is necessary to derive a flow accumulation map and slope angle map. The flow accumulation map represents accumulated flow as the accumulated

weight of all cells flowing into each downslope cell in the output raster. The stream power index map was derived using the Raster calculator implemented in ArcGIS 10.8. following the equation proposed by Moore et al. (1991):

$$\text{SPI} = \ln(\text{flow accumulation}) \times \frac{\text{slp}}{100} \quad (2)$$

where flow accumulation is the value of each cell on the flow accumulation map and,  $\text{slp}$  is the slope map in degrees derived from the LiDAR DTM. The final SPI map was classified into four categories using the quantile classification method.

High-resolution digital orthophoto images of 0.5 m resolution for different periods are available via Web Map

Service (WMS) on The Geoportal of the State Geodetic Administration (SGA). Orthophoto images used for interpretation of badland areas and verification of visual interpreted landslides based on LiDAR data is from 2020.

## 4 Results

Visual identification and mapping of landform features were made on the study area (20 km<sup>2</sup>) at a large scale (1:500) to produce detailed landslide and erosion inventory maps for implementation in the spatial planning system. After a preliminary visual interpretation of LiDAR DTM and field verifications, it was concluded that four types of landforms could be mapped, i.e. badlands, gully and combined erosion, unstable slopes, and landslides.

### 4.1 Badlands

Badlands were identified and mapped starting from the orthophoto images (year 2020, resolution 0.5 m) available for the territory of the Republic of Croatia on the State Geodetic Administration website. The badland areas were identified as landforms with sparse or no vegetation in the surrounding areas. In addition, most of the badlands in the study area are characterised by a sandstone cap, representing an erosive base level. The boundary of the badland-affected slope was additionally mapped in detail on the LiDAR DTM derivatives, i.e. a combination of hillshade map, 65% transparent slope map and 1 m contour map. Differences between orthophoto and LiDAR interpretation were significant (Fig. 4), on some locations, the difference was up to 20 m. The unique ID, type of badlands and the total area covered by the erosion process were associated with each mapped landform. There are three morphological types of badland areas in the study area, following the classification developed by Moretti and Rodolfi (2000). Type “A” develops because of the action of concentrated water runoff and results in sharp and dissected landforms, very dense drainage patterns and deep V-shaped channels. Type “B” is mainly due to superficial slides of soil or regolith on the unweathered substratum, resulting in gentler slopes and less dense drainage patterns, i.e. it represents a natural evaluation of type A badlands due to landform smoothing and vegetation growth (Ciccacci et al. 2008). Type “AB” is an intermediate landform between Type A, where the dominant process is vertical erosion, and Type B, where superficial sliding prevails. Classification of each mapped badlands area was performed based on LiDAR data derivatives because shadows on orthophoto images disabled the possibility of identifying the degree of landform dissection and drainage network density.

### 4.2 Gully and Combined Erosion

Based on the LiDAR DTM derivatives, the identification and detailed mapping of different types of soil erosion processes is widely used (Vanmaercke et al. 2021). The whole methodology for the identification and mapping of a gully, combined, and sheet erosion using the visual interpretation of high-resolution LiDAR DTM is presented in Đomlija et al. (2019) and Jagodnik et al. (2020). Furthermore, Đomlija et al. (2019) proved that only gully and combined erosion phenomena could be mapped with a high geographical and thematic accuracy using LiDAR data. Sheet erosion, however, can only be indirectly identified on certain LiDAR DTM derivatives based on the recognition of colluvial deposits accumulated at the foot of the eroded slopes. Considering the potential of high-resolution LiDAR data for soil erosion mapping, only gully and combined erosion were mapped in the study area. Gullies with a width of more than 3 m and wider areas affected by combined erosion were mapped by a single polygon (Fig. 5).

Gully erosion was easily recognised due to the elongated or branchy shape of gully channels on hillshade, slope and SPI maps. The SPI approximates the potential locations and magnitude of the gully formation, and higher values of the SPI indicate a high erosional capacity, while lower values indicate ridges. The wider area affected by combined erosion can be precisely delineated based on the disturbed slope surface appearance on the hillshade map, the small-sized drainage networks on the SPI map and the rough surface on the SAR maps. Furthermore, all areas identified as combined erosion are located within the relief concavities, with gullies formed in their central parts. The rough texture of the affected areas (Fig. 5b) distinguishes the soil erosion area from the surroundings, while the highest values are assigned to badland areas. A high level of precision in mapping the gully and combined erosion phenomena was achieved by drawing the separate portions of polygons based on the visual analysis of different LiDAR DTM derivatives and subsequent merging of drawn lines into a unique polygon while mapping.

### 4.3 Unstable Slopes

Unstable slopes were categorised as areas with different types of landslide mechanisms on the artificial slopes (Fig. 6). During intense rainfall events, there are a large number of slope movement processes on the artificial slopes along the roads, including superficial sliding, falling and toppling. Examples of slope movements on unstable slopes along the roads after extreme rainfall events in December 2020 are shown in Fig. 2c, d. Furthermore, most of these slope instabilities have a small volume that can be removed quickly

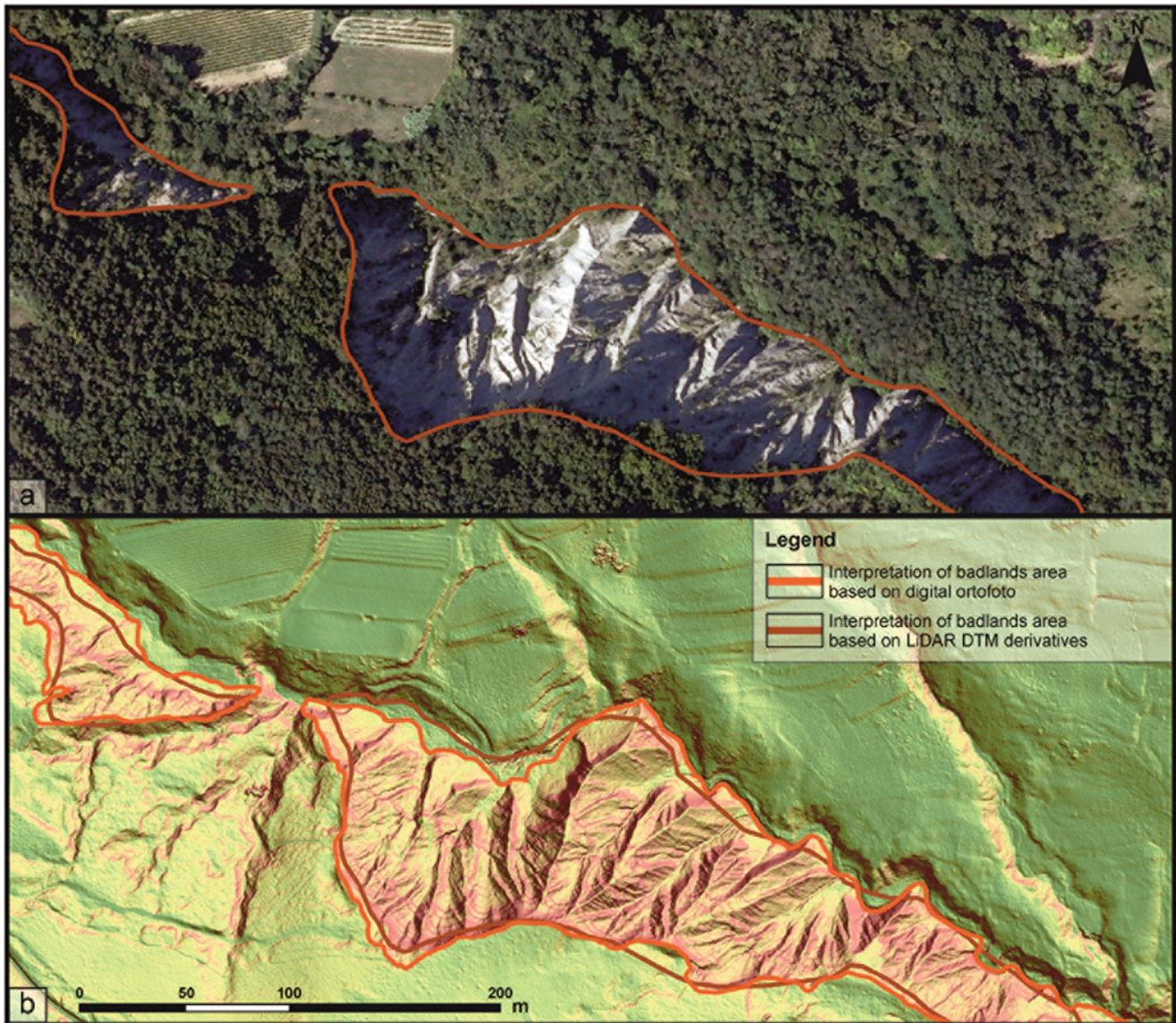


**Fig. 4** Badland inventory mapping: (a) interpretation based on digital orthophoto map; (b) interpretation based on LiDAR DTM derivatives

after initiation during emergency road maintenance. Considering the removal of colluvium from the roads, most of the landslide phenomena on artificial slopes will not be visible on LiDAR DTM derivatives unless laser scanning is recorded immediately after the landslide event. Furthermore, if visible on the LiDAR DTM derivatives, the exact landslide boundaries could not be mapped due to the coalescence of superficial landslides or poor contrast between affected and unaffected areas due to the intense erosion.

#### 4.4 Landslides

Landslide identification on the LiDAR DTM morphometric derivatives (Fig. 7) is based on recognising landslide features (e.g., concave main scarps, hummocky landslide bodies and convex landslide toes). A digital orthophoto map from 2020 (Fig. 7a) was used during landslide identification to check the morphological forms along roads and houses, such as artificial fills and cuts, which can have a similar appearance to landslides on DTM derivatives. Each mapped landslide polygon was assigned with the landslide type and certainty of

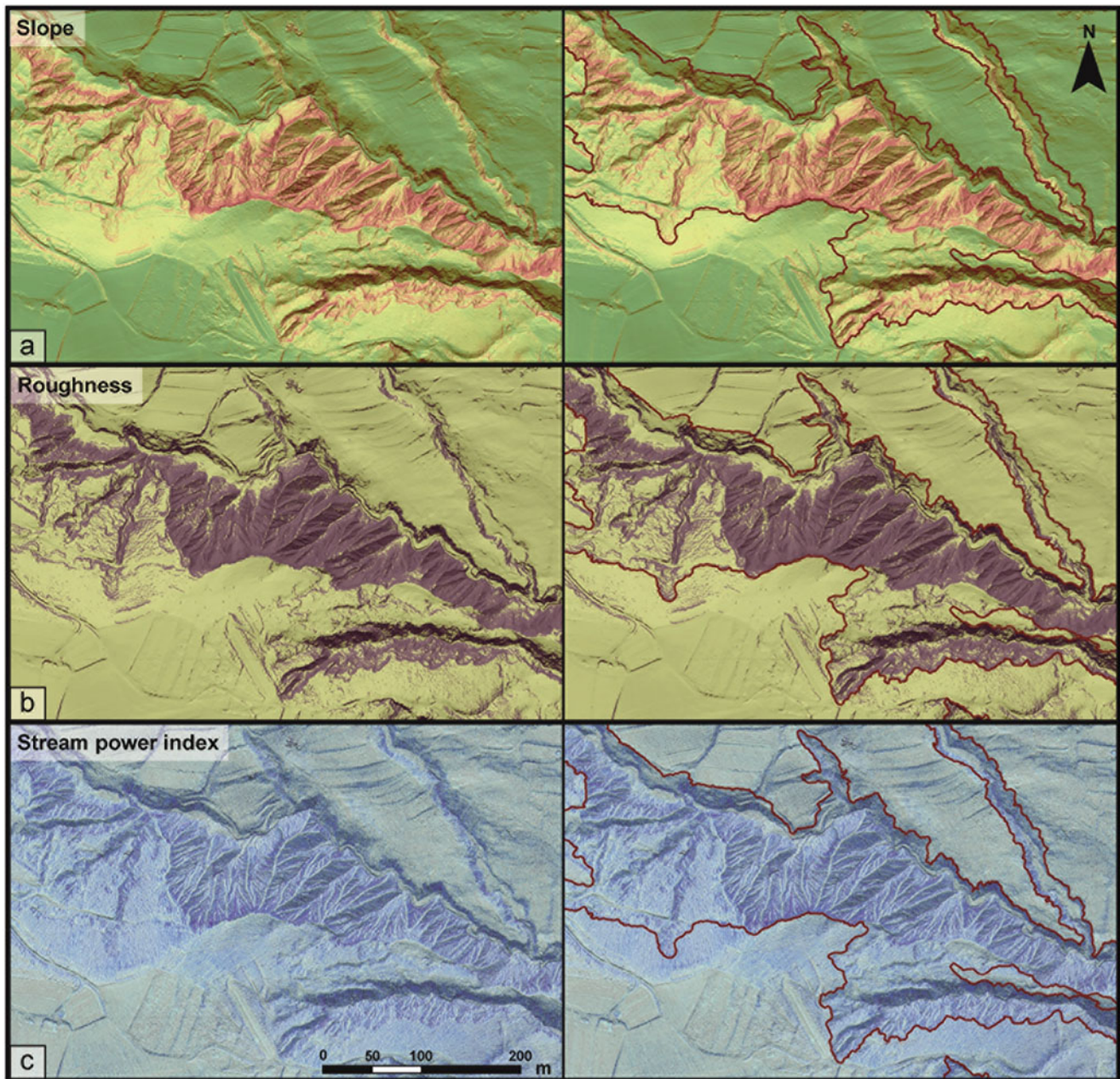


**Fig. 5** Gully and combined erosion inventory mapping: (a) interpretation on transparent slope map over hillshade map; (b) interpretation on transparent SAR map; (c) interpretation on transparent SPI map

mapping, e.g., accuracy and precision. The certainty of landslide identification was expressed as ‘high certainty’ where the landslide parts and morphology are clearly visible and easy to identify and ‘low certainty’ where the landslide parts are not clearly visible or are missing, and the landslide morphology is unclear, i.e., landslide identification is not with high reliability. The precision of mapping was expressed as ‘high precision’ where the landslide boundaries (crown, flanks, and toe) are clearly visible, and landslide mapping can be performed with high spatial accuracy; and ‘low precision’

where the landslide boundaries are smooth and unclear, i.e. where landslides are assumed based on a zone of depression/ accumulation and landslide boundary mapping is with low spatial accuracy.

At the beginning of the landslide inventory mapping process, Lukačić et al. 2022 conducted research in which seven landslide researchers interpreted landslides on LiDAR data on a small part of the study area (0.3 km<sup>2</sup>). Landslide researchers had different levels of LiDAR mapping experience and knowledge of the study area. The results were



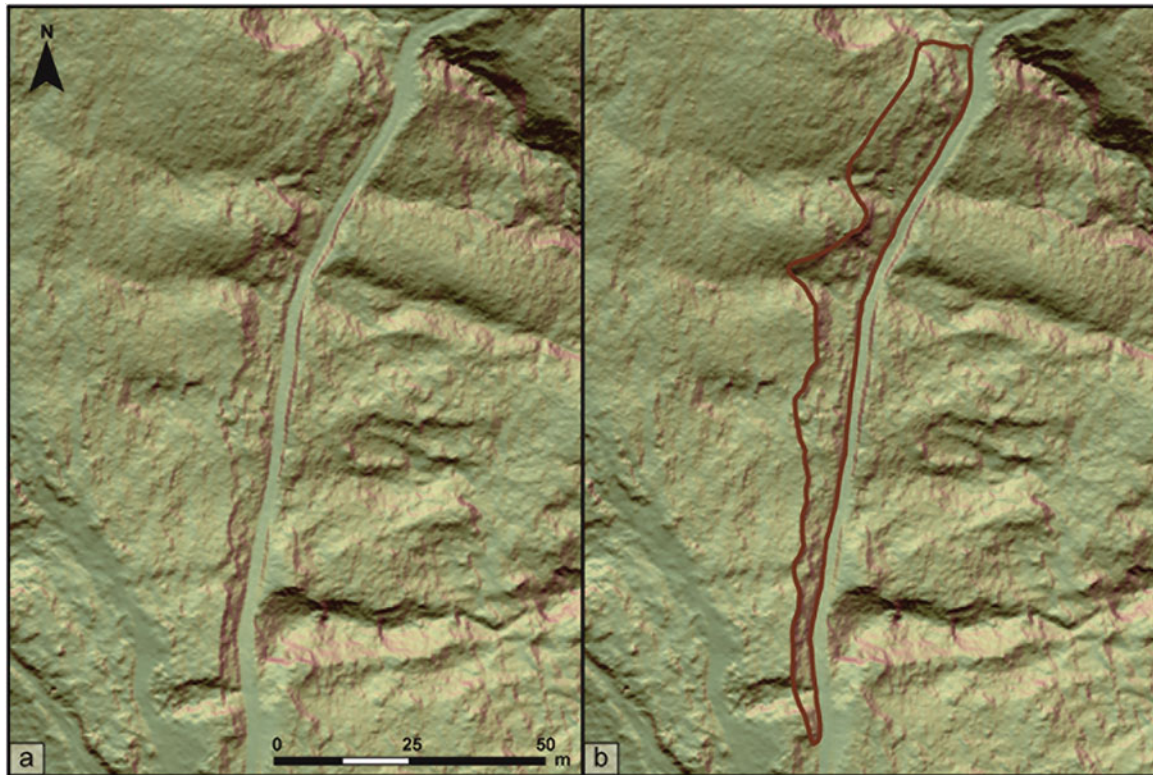


**Fig. 6** Interpretation of unstable slopes based on LiDAR DTM derivatives, i.e. hillshade and slope map

significant differences in LiDAR interpretation among landslide experts (Fig. 8), which did not depend on previous knowledge of the study area, but on the experience and skill of interpreting LiDAR data. The final matching of landslide inventories produced by eight experts was less than 30%. Furthermore, obtained results show that the same pilot area must be mapped multiple times to accomplish a high-accuracy landslide inventory map (Lukačić et al. 2022). Landslide inventory mapping was back and forth between LiDAR interpretation in the cabinet and field verification because it was necessary to calibrate mapping skills in the Istrian flysch terrains. During the field verification, the number of unconfirmed and confirmed landslides with modified landslide boundaries indicated that the common recommendation about verifying 10% of landslides in the landslide inventory (Galli et al. 2008) is not sufficient in the pilot area with complex geology settings and multi-hazard processes. Therefore, to ensure the accuracy of the landslide inventory map, it is necessary to increase the ratio of field-verified and confirmed landslides related to the total number of landslides in an inventory map (Lukačić et al. 2022).

The biggest challenge was landslide identification and mapping in the affected by gully and combined erosion and badland areas (Fig. 9). Every inch of erosion-affected area is disturbed due to the slope processes, and because of that, it

was very hard to distinguish sliding from erosion processes on LIDAR DTM derivatives. Furthermore, due to the higher certainty of the final landslide inventory, only landslides with clearly visible depression and accumulation zones were mapped in soil erosion areas.

## 5 Application in the Spatial Planning System

Detailed landslide and soil erosion inventory maps (M 1:500) of the study area (20 km<sup>2</sup>) in Istrian flysch-type rocks consist of four types of landforms, i.e. badlands, gully and combined erosion, unstable slopes, and landslides (Fig. 10a). Potential users of landslide and soil erosion inventory data and information differ widely (Wold et al. 1989), although they can be divided in four general categories are (1) scientists and engineers who use the information directly; (2) planners and decision-makers who consider landslide hazards among other land-use and development criteria; (3) developers, builders, and financial and insuring organisations; and (4) interested citizens, educators, and others with little or no technical experience. The main purpose of derived inventories is an implementation in the spatial planning system and application in further large-scale landslide

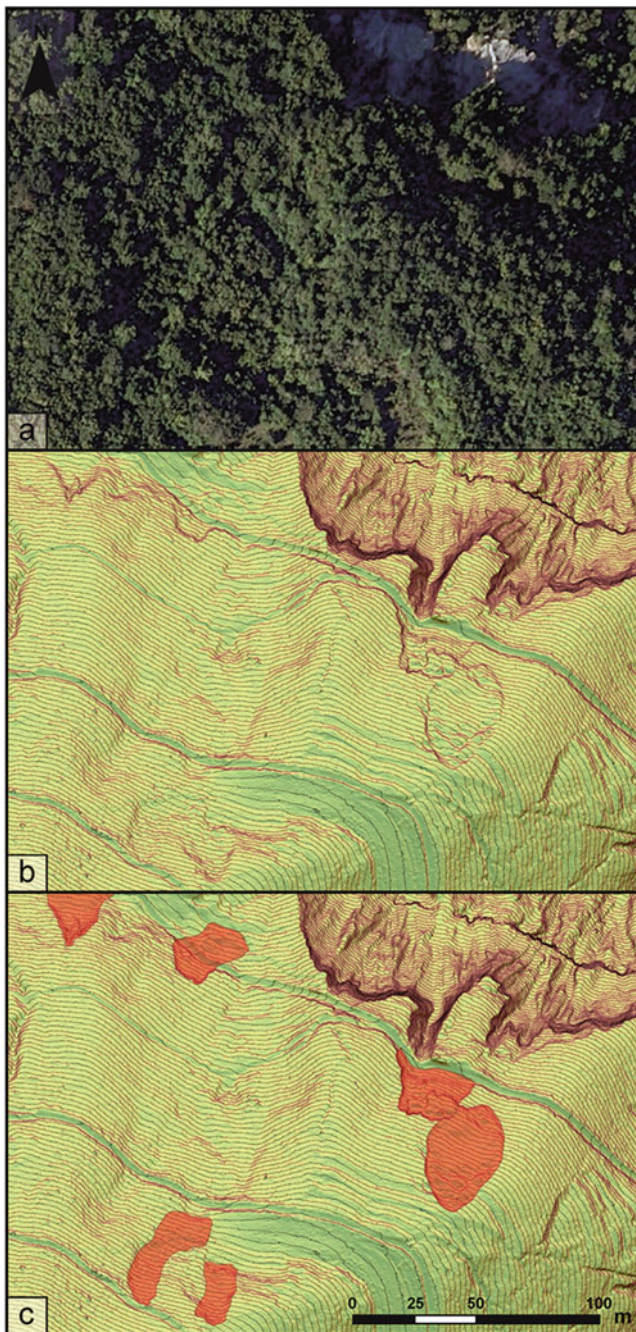


**Fig. 7** Landslide inventory mapping based on LiDAR DTM derivatives, i.e. hillshade, slope and contour map

susceptibility assessment. Inventory maps could be used to manage landslide and soil erosion hazards in populated areas by excluding development or by proposing requirements for minimum on-site geotechnical investigations in the frame of slope stability assessment before constructing in areas endangered by registered landslides or soil erosion processes. The approach of avoiding erosion and landslide-prone areas is rarely feasible, and it is neither possible nor desirable to proscribe development in any urbanised area. However, the

USGS proposal for a national landslide hazards mitigation strategy (Spiker and Gori 2000) summarises the major mitigation approaches, including: (1) restricting development in landslide-prone areas; (2) enforcing codes for excavation, construction, and grading; (3) engineering for slope stability; (4) deploying monitoring and warning systems; and (5) providing landslide insurance.

Based on the USGS strategy, we defined two zones with measures applicable to spatial plans at the local level. The first zone was determined based on the extent of badland areas and includes restricting development, i.e., a ban on expanding construction areas in the badlands areas. The second zone includes areas affected by gully and combined erosion and shallow landslides, in which a spatial plan measure enforces codes for excavation and construction. In Fig. 10b it is shown an example of zoning based on the close-up extent of derived landslide and erosional landslide inventory.

Regardless of restricting development in badland areas, several badlands areas in central Istria have a large potential as geotourism sites because of their often great esthetical value or picturesque nature. Furthermore, if well managed, gullies can become productive and biodiverse hotspots that play a key role as ecological corridors (Romero-Díaz et al. 2019).

## 6 Discussion and Conclusion

The findings of this study inform which LiDAR-based morphometric maps are the most effective in providing geomorphological clues and which landslide and erosion processes can be identified and mapped with high geographical and thematic accuracy using high-resolution remote sensing data. Furthermore, the proposed methodology for accurately identifying and detailed inventory mapping of badlands, gully and combined erosion, unstable slopes and landslides on a large scale can be used as guidance in future studies in areas with similar geological settings and degree of urbanisation.

Although the visual interpretation of LiDAR DTM derivatives and manual mapping of landslide and soil erosion landforms is time-consuming, it is considered that the same quality of the results could not be obtained by using the conventional geomorphological mapping methods, given the specific topographic characteristics of the studied area, i.e. inaccessible and densely vegetated area. Furthermore, the possibilities of using the automated landslide and soil erosion mapping methods are limited regarding the numerous artificial traces on the affected surface that are not topographic signatures of geomorphological processes. However, the possibilities of visual recognition of landslide and soil erosion phenomena, and thus the quality of the mapping results,

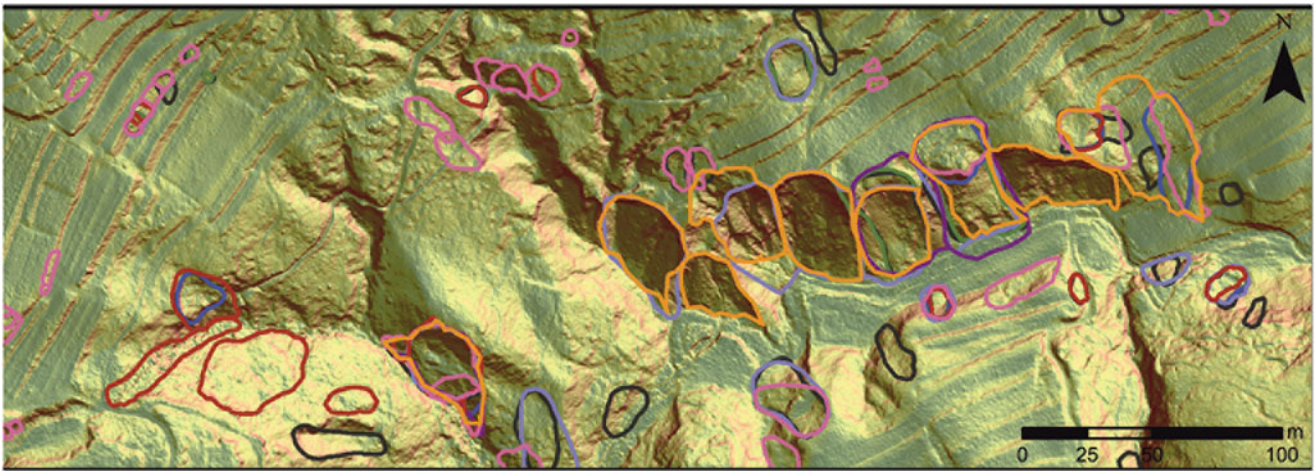


**Fig. 8** Result of visual landslide interpretation carried out by seven landslide experts with different LiDAR mapping experience and knowledge of the study area

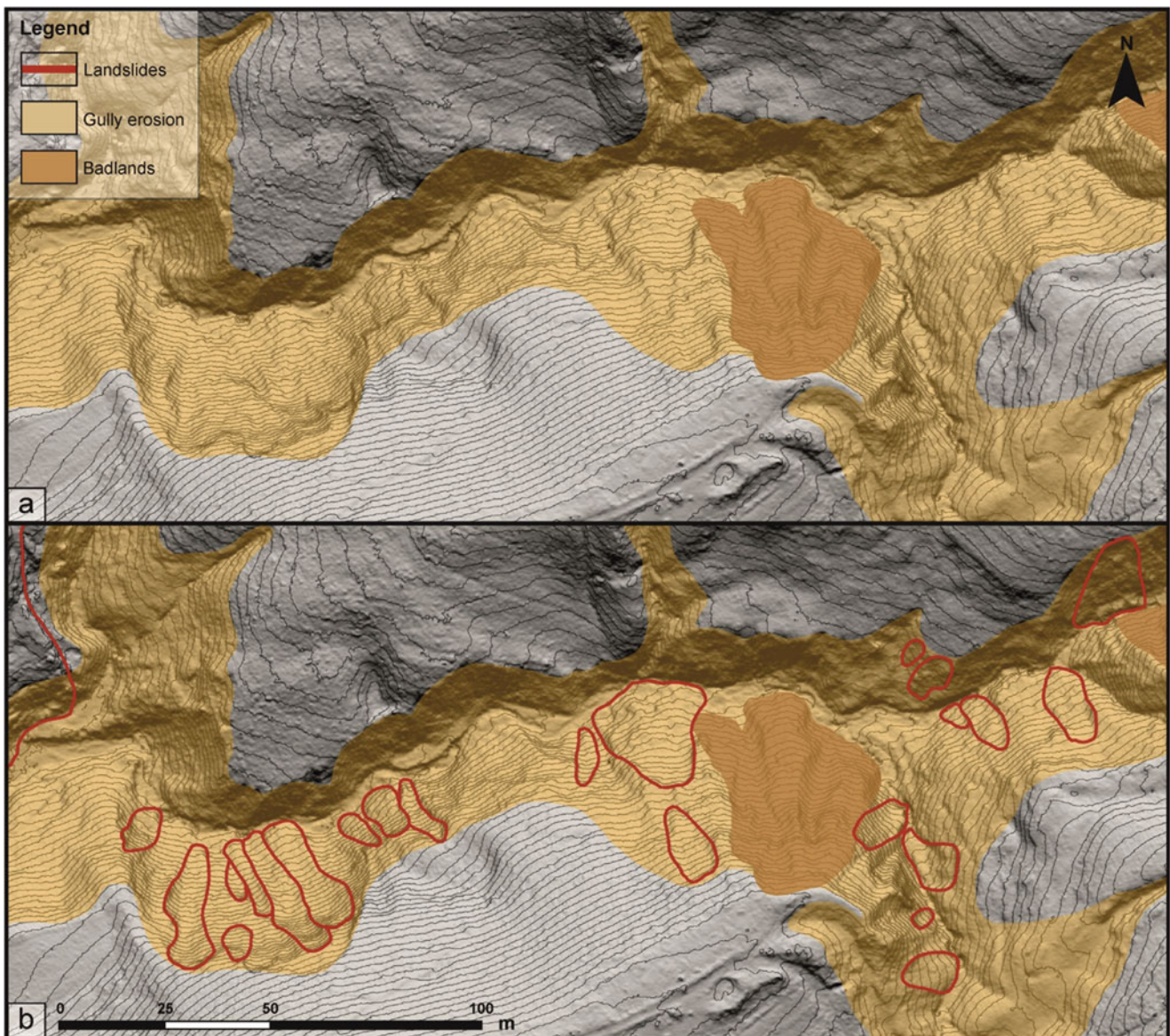


**Fig. 9** Example of landslide mapping in areas affected by gully and combined erosion on LiDAR DTM derivatives

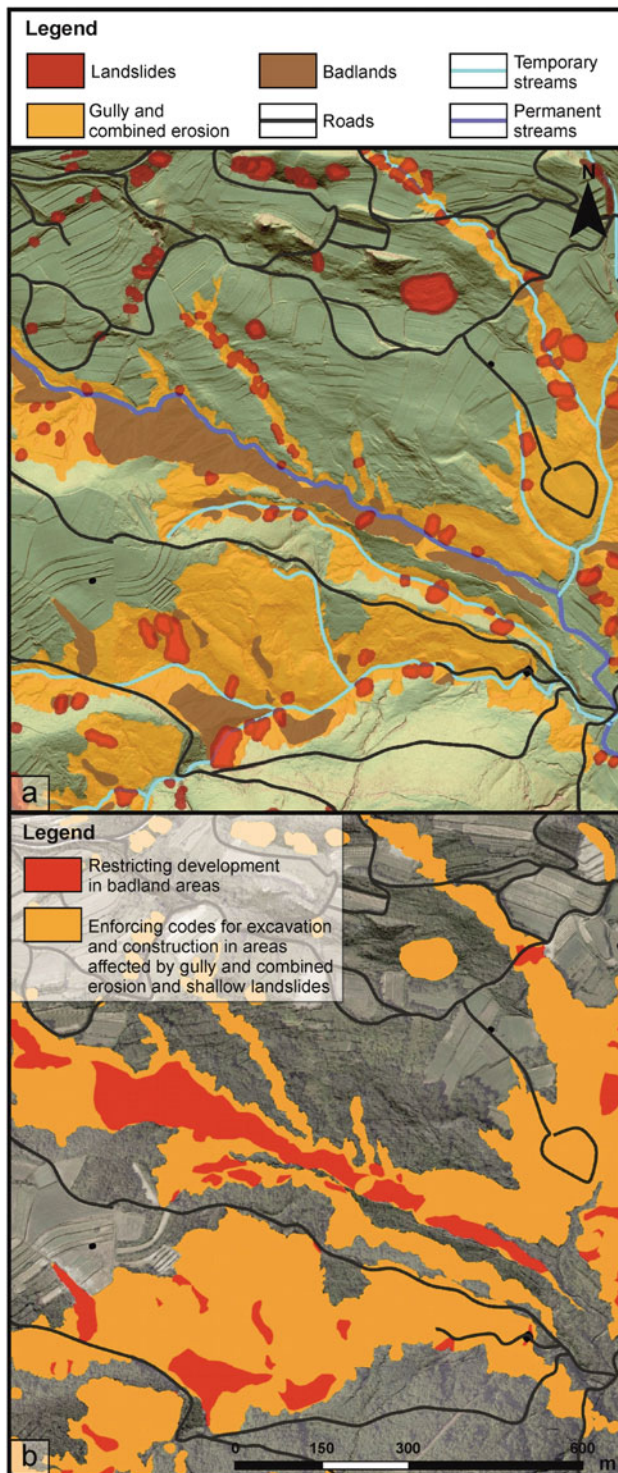


**Fig. 10** Application of landslide and soil erosion inventory maps in the spatial planning system: (a) close-up extent of final inventory map; (b) derived map with defined spatial plan measures

strongly depends on the spatial resolution of used remote sensing data and researcher experience in interpreting LiDAR DTM derivatives because accurate and precise delineating of the landforms can be complex mapping

challenge. By analysing inventory completeness and size of mapped landforms, we can estimate the quality of LiDAR-derived inventory maps (Bernat Gazibara et al. 2019a, b). Therefore, the LiDAR-base landslide and erosion inventory maps prepared using the proposed mapping procedure are usually considered sustainably complete for future applications, such as landslide and erosion susceptibility assessment or estimating temporal changes in gully erosion. Furthermore, a detailed inventory map derived based on visual interpretation of high-resolution remote sensing data, combined with landslide and soil erosion susceptibility maps, provides appropriately detailed input data for defining measures in local-level spatial plans. Derived inventory maps can be used to manage landslide and soil erosion hazards in populated areas by restricting development in badland areas or enforcing codes for excavation and construction in areas endangered by registered landslides or gully and combined erosion processes.

**Acknowledgments** This research has been fully supported by the Croatian Science Foundation under the project methodology development for landslide susceptibility assessment for and use planning based on LiDAR technology, LandSlidePlan (HRZZ IP-2019-04-9900, HRZZ DOK-2020-01-2432).

## References

- Arbanas Ž, Benac Č, Jardas B (1999) Small landslides on the flysch of Istria. In: Proceedings of the 3rd conference of Slovenian geotechnical society. SloGeD, Ljubljana, pp 81–88
- Arbanas Ž, Benac Č, Jurak V (2006) Causes of debris flow formation in flysch area of North Istria, Croatia. In: Monitoring, simulation, prevention and remediation of dense and debris flows. WIT Press, Rhodes, pp 283–292
- Arbanas Ž, Mihalić S, Grošić M et al (2010) Brus Landslide, translational block sliding in flysch rock mass. In: Zhao J, Labiouse V, Dudt J-P, Mathier J-F (eds) Proceedings of the European rock mechanics symposium (Eurock 2010). CRC Press/Balkema, Laussane, London, pp 635–638
- Arbanas Ž, Jovančević SD, Vivoda M, Arbanas SM (2014) Study of landslides in flysch deposits of North Istria, Croatia: landslide data collection and recent landslide occurrences. In: Sassa K, Canuti P, Yin Y (eds) Landslide science for a safer Geoenvironment. Springer International Publishing, Cham, pp 89–94
- Ardizzone F, Cardinali M, Galli M et al (2007) Identification and mapping of recent rainfall-induced landslides using elevation data collected by airborne Lidar. *Nat Hazards Earth Syst Sci* 7:637–650. <https://doi.org/10.5194/nhess-7-637-2007>
- Bergant S, Tišljarić J, Šparica M (2003) Eocene Carbonates and Flysch Deposits of the Pazin Basin. In: Vlahović I, Tišljarić J (eds) Field trip guidebook: evolution of depositional environments from the palaeozoic to the quaternary in the Karst Dinarides and the Pannonian Basin. Institut za geološka istraživanja, Opatija, Zagreb, pp 57–64
- Bernat Gazibara S, Krkač M, Mihalić Arbanas S (2019a) Verification of historical landslide inventory maps for the Podsljeme area in the City of Zagreb using LiDAR-based landslide inventory. *Rudarsko-geološko-naftni zbornik* 34(1):45–58. <https://doi.org/10.17794/rgn.2019.1.5>

- Bernat Gazibara S, Krkač M, Mihalić Arbanas S (2019b) Landslide inventory mapping using LiDAR data in the City of Zagreb (Croatia). *J Maps* 15:773–779. <https://doi.org/10.1080/17445647.2019.1671906>
- Bernat Gazibara S, Mihalić Arbanas S, Sinčić M, et al (2022) LandSlidePlan -scientific research project on landslide susceptibility assessment in large scale. In: Proceedings of the 5th regional symposium on landslides in Adriatic-Balkan region. Faculty of Civil Engineering, University of Rijeka and Faculty of mining, geology and petroleum engineering, University of Zagreb, Rijeka, Croatia
- Berry JK (2002) Use surface area for realistic calculations. *Geoworld* 15(9):1–20
- Ciccacci S, Galiano M, Roma MA, Salvatore MC (2008) Morphological analysis and erosion rate evaluation in badlands of Radicofani area (southern Tuscany — Italy). *Catena* 74:87–97. <https://doi.org/10.1016/j.catena.2008.03.012>
- Domlija P, Bernat Gazibara S, Arbanas Ž, Mihalić Arbanas S (2019) Identification and mapping of soil erosion processes using the visual interpretation of LiDAR imagery. *IJGI* 8:438. <https://doi.org/10.3390/ijgi8100438>
- Dugonjić Jovančević S, Arbanas Ž (2012) Recent landslides on the Istrian peninsula, Croatia. *Nat Hazards* 62:1323–1338. <https://doi.org/10.1007/s11069-012-0150-4>
- Eeckhaut MVD, Poesen J, Verstraeten G et al (2007) Use of LIDAR-derived images for mapping old landslides under forest. *Earth Surf Process Landforms* 32:754–769. <https://doi.org/10.1002/esp.1417>
- Galli M, Ardizzone F, Cardinali M et al (2008) Comparing landslide inventory maps. *Geomorphology* 94:268–289. <https://doi.org/10.1016/j.geomorph.2006.09.023>
- Gulam V, Pollak D, Podolszki L (2014) The analysis of the flysch badlands inventory in Central Istria, Croatia. *Geol Cro* 67:1–15. <https://doi.org/10.4154/GC.2014.01>
- Guzzetti F, Cardinali M, Reichenbach P, Carrara A (2000) Comparing landslide maps: a case study in the upper Tiber River basin, Central Italy. *Environ Manag* 25:247–263. <https://doi.org/10.1007/s002679910020>
- Guzzetti F, Mondini AC, Cardinali M et al (2012) Landslide inventory maps: new tools for an old problem. *Earth Sci Rev* 112:42–66. <https://doi.org/10.1016/j.earscirev.2012.02.001>
- Jagodnik P, Bernat Gazibara S, Arbanas Ž, Mihalić Arbanas S (2020) Engineering geological mapping using airborne LiDAR datasets – an example from the Vinodol Valley, Croatia. *J Maps* 16:855–866. <https://doi.org/10.1080/17445647.2020.1831980>
- Jenness J (2007) Some thoughts on analyzing topographic habitat characteristics
- Lukačić H, Bernat Gazibara S, Sinčić M, et al (2022) Influence of expert knowledge on completeness and accuracy of landslide inventory maps – example from Istria, Croatia. In: Proceedings of the 5th regional symposium on landslides in Adriatic-Balkan region. Faculty of Civil Engineering, University of Rijeka and Faculty of mining, geology and petroleum engineering, University of Zagreb, Rijeka, Croatia
- Mihalić S, Arbanas Ž, Krkač M, Dugonjić S (2011) Analysis of sliding hazard in wider area of Brus landslide. In: Anagnostopoulos A, Pachakis M, Tsatsanifos C (eds) Proceedings of the XV European conference on soil mechanics and geotechnical engineering. IOS Press, Atena, Amsterdam, pp 1377–1382
- Moore ID, Grayson RB, Ladson AR (1991) Digital terrain modelling: a review of hydrological, geomorphological, and biological applications. *Hydrol Process* 5:3–30. <https://doi.org/10.1002/hyp.3360050103>
- Moretti S, Rodolfi G (2000) A typical “calanchi” landscape on the eastern Apennine margin (Atri, Central Italy): geomorphological features and evolution. *Catena* 40:217–228. [https://doi.org/10.1016/S0341-8162\(99\)00086-7](https://doi.org/10.1016/S0341-8162(99)00086-7)
- Pleničar M, Polšak A, Šikić D (1969) Basic geological map, scale 1: 100,000, Trst, Sheet 33–88
- Romero-Díaz A, Díaz-Pereira E, De Vente J (2019) Ecosystem services provision by gully control. A review. *CIG* 45:333–366. <https://doi.org/10.18172/cig.3552>
- Sinčić M, Bernat Gazibara S, Krkač M et al (2022) The use of high-resolution remote sensing data in preparation of input data for large-scale landslide Hazard assessments. *Land* 11:1360. <https://doi.org/10.3390/land11081360>
- Spiker EC, Gori PL (2000) National Landslide Hazards Mitigation Strategy: a framework for loss reduction. U.S. Dept. of the Interior, U.S. Geological Survey
- UN (2015) Sendai framework for disaster risk reduction 2015–2030. UN, Geneva
- van Westen CJ, van Asch TWJ, Soeters R (2006) Landslide hazard and risk zonation—why is it still so difficult? *Bull Eng Geol Environ* 65:167–184. <https://doi.org/10.1007/s10064-005-0023-0>
- Vanmaercke M, Panagos P, Vanwallegghem T et al (2021) Measuring, modelling and managing gully erosion at large scales: a state of the art. *Earth Sci Rev* 218:103637. <https://doi.org/10.1016/j.earscirev.2021.103637>
- Vivoda Prodan M, Arbanas Ž (2016) Weathering influence on properties of siltstones from Istria, Croatia. *Adv Mater Sci Eng* 2016:1–15. <https://doi.org/10.1155/2016/3073202>
- Wold RL, Jochim CL, Agency USFEM, Survey CG (1989) Landslide loss reduction: a guide for state and local government planning. Federal Emergency Management Agency, Washington, DC

**Open Access** This chapter is licensed under the terms of the Creative Commons Attribution 4.0 International License (<http://creativecommons.org/licenses/by/4.0/>), which permits use, sharing, adaptation, distribution and reproduction in any medium or format, as long as you give appropriate credit to the original author(s) and the source, provide a link to the Creative Commons license and indicate if changes were made.

The images or other third party material in this chapter are included in the chapter's Creative Commons license, unless indicated otherwise in a credit line to the material. If material is not included in the chapter's Creative Commons license and your intended use is not permitted by statutory regulation or exceeds the permitted use, you will need to obtain permission directly from the copyright holder.

